Desalination and Water Treatment
www.deswater.com

doi: 10.5004/dwt.2017.21021

80 (2017) 18–26
June

The influences of deposited silica nanoparticles on a forward osmosis membrane

Youngpil Chun[a,b], Dennis Mulcahy[a], In S. Kim[c], Linda Zou[d,*]

[a]*Natural and Built Environments Research Centre, School of Natural and Built Environments, University of South Australia, Mawson Lakes, South Australia, Australia, emails: youngpil.chun@mymail.unisa.edu.au (Y. Chun), dennis.mulcahy@unisa.edu.au (D. Mulcahy)*
[b]*Singapore Membrane Technology Centre, Nanyang Environment & Water Research Institute, Nanyang Technological University, Singapore, Singapore*
[c]*Global Desalination Research Center, School of Environmental Science and Engineering, Gwangju Institute of Science and Technology, Gwangju, Korea, email: iskim@gist.ac.kr*
[d]*Department of Chemical and Environmental Engineering, Khalifa University of Science and Technology, Masdar Institute, Masdar City, Abu Dhabi, UAE, Tel. +971 2 810 9304; email: lyuanzou@masdar.ac.ae*

Received 21 March 2017; Accepted 5 June 2017

ABSTRACT

The effect of silica nanoparticles (SNPs) deposition on the properties of a commercial forward osmosis (FO) membrane was investigated in this work. Deposition of SNPs on the FO membrane was performed by a conventional sol–gel hydrolysis of tetraethyl orthosilicate and a simple dip-coating procedure. Scanning electron microscopy, X-ray photoelectron spectroscopy and attenuated total reflectance–Fourier transform infrared spectroscopy confirmed the successful deposition of SNPs on the membrane surface. The coated membranes were used in a bench scale FO system and their performance was evaluated through measuring the permeate water flux and fouling resistance. Successful deposition of SNPs smoothed out the membrane surface and increased surface hydrophilicity. The effects of SNP enabled a higher water flux and fouling resistance than for the pristine FO membrane, possibly due to increased hydrophilicity and decreased membrane roughness.

Keywords: FO membrane; Membrane coating; Sol–gel hydrolysis; Silica nanoparticles; Membrane fouling

1. Introduction

Osmotically driven membrane processes (ODMPs) including forward osmosis (FO) and pressure retarded osmosis have been extensively studied in the last decade to address global water and energy issues [1–3]. The applications of ODMP have been exponentially expanded to various water purification technologies such as brackish/seawater desalination, water treatment and wastewater reclamation [2]. Although ODMP shows great promise to tackle the water and energy issues, fouling is still one of the significant limiting factors and is unavoidable in the processes [3–5]. Thus, the development of antifouling membranes is required for sustainable membrane process operation.

Research has been focused on enhancing membrane performances including the antifouling properties of the membrane. A novel organic–inorganic hybrid membrane can provide a synergy between the traditional benefits of membrane polymers and unique properties of inorganic nanomaterials [6]. Incorporation of inorganic nanomaterials such as SiO_2 [7,8], TiO_2 [9,10], $AgNO_3$ [11–13], Al_2O_3 [14,15] and $Mg(OH)_2$ [16] into polymeric membranes has been extensively explored for improved membrane performance in terms of permeability, thermal stability, mechanical strength or better control of the membrane surface characteristics and fouling mitigation. These hybrid polymer/inorganic material membranes can

* Corresponding author.

be prepared by either direct deposition of inorganic nanomaterials onto the membrane surface or by blending into the active layer (thin film) during the membrane fabrication processes (i.e., phase inversion and interfacial polymerisation) [17]. Inorganic nanoparticles in sol–gel can also be applied to membrane selective and/or substrate layers by various methods, dip-coating and spin-coating are the two most common coating methods, others include the recently emerged spraying and electrodeposition techniques [18]. Successful in situ formation of silver nanoparticles (Ag-NPs) and copper-based nanoparticles (Cu-NPs) onto reverse osmosis (RO) membranes have been demonstrated biofouling mitigation via facile in situ coating techniques [15,19].

In the present study, the commercial FO membrane was dip-coated using silica nanoparticles (SNPs) as a simple and straightforward technique. Silica was selected based on its low cost and lower environmental toxicity compared with other nanomaterials such as ZnO and TiO_2 [20–22]. Silica materials have also been widely used due to their structural flexibility, stability and hydrophilic properties in order to enhance water permeability, hydrophilicity and antifouling property [22,23]. Jadav and Singh [7] fabricated a porous polysulphone (PSF) support layer using polyamide and SNPs via interfacial polymerisation to produce a thin-film nanocomposite (TFN) membrane. The TFN membranes containing about 1–2 wt% showed the best performance in terms of separation efficiency and permeate flux. The water flux increased with increase in the silica content of the TFN membranes; however, the NaCl rejection was the highest in the membrane with silica content 1–2 wt%. Liu and Ng [24] successfully fabricated a thin-film composite (TFC) FO membrane using a different loading of the nano-sized silica–PSF mixed matrix substrate. The best performing membrane showed increased hydrophilicity and a reduced structural parameter (S) value and the effect of the internal concentration polarisation (ICP) was decreased. Thus, the membrane tripled water flux compared with the control membrane without compromising on the reverse salt flux.

In this study, a commercially available FO membrane was coated using SNPs via a facile sol–gel process and coating procedure without the issues associated with a high temperature and complex and costly fabrication process. The physicochemical surface characteristics of the modified membrane were investigated. The surface modified membrane (SNPM) was also used to evaluate the water flux and fouling behaviours.

2. Materials and methods

2.1. Membrane coating

Tetraethyl orthosilicate (TEOS, reagent grade, 98%), hydrochloric acid (HCl, ACS grade, 37%), isopropyl alcohol (≥99.7%) and ethanol (ACS grade, ≥99.5%) were obtained from Sigma-Aldrich (USA). Polyamide TFC FO membranes (Hydration Technology Inc., USA) were used for surface modification. 130 mL of 7.6% (w/v) TEOS in isopropanol was added dropwise to 610 mL of 0.2 N HCl solution with constant stirring at room temperature. The solution was then kept covered and undisturbed for 4 d to undergo hydrolysis for production of the SNPs [7]. The membrane (both sides) was dipped in the final solution for 24 h and then dried for 24 h in the air at room temperature. The optimal soaking time in this study was chosen after repeated trials based on the water flux value. The concentrations of the SNPs were kept the same so as to solely focus on the effect of deposited SNPs on the FO membrane performance compared with the pristine membrane. The SNPMs were stored in MilliQ water (Millipore, USA) at 4°C for at least 24 h.

2.2. Membrane surface characterisation

The morphology, topography and physicochemical properties of pristine and SNPMs were characterised, respectively. Contact angle measurements were carried out with a contact angle goniometer (Phoenix, Surface Electro Optics, Korea) by the captive bubble method in ambient condition.

Field emission scanning electron microscopy (FESEM; JSM-7500F, JEOL, Japan) was used to examine the morphology of the membrane. An energy dispersive spectrometer (EDS; EDAX Genesis, JEOL, Japan) was used for the elemental composition of the pristine and SNPMs.

X-ray photoelectron spectroscopy (XPS; VG Multilab 2000, Thermo VG Scientific, UK) was used to characterise membrane elemental composition and chemical binding before and after the SNP coating. The survey scans were performed over 0–1,200 eV binding energy in 0.500 eV steps.

Atomic force microscopy (AFM; XE-100, PSIA, Korea) and a non-contact cantilever (NCHR 10 M, Park Systems, Korea) were used to obtain the topographical images of the membrane surface. The scanning area was 10 μm^2. The values of mean roughness (R_a) were derived from the AFM images.

An attenuated total reflectance–Fourier transform infrared (ATR–FTIR) spectrometer (FT/IR-6100, JASCO, Japan) was used to examine the chemical structure of the pristine and SNPM after SNPs were deposited. The air background of the instrument was run for each sample. The spectrum of each sample was collected between wavelengths 4,000 and 600 cm^{-1}.

2.3. FO performance tests

In order to evaluate the improvement in the FO performance, a bench-scale FO membrane system was set up as described in the previous study [25]. The effective membrane dimension of the FO module was 77 mm in length by 26 mm in width by 3 mm in height. The feed and draw solutions were co-currently flowed using a gear pump drive (Model 7527-15, Cole-Parmer, USA) on both sides, with the flow rate of 500 mL/min (25.48 cm/s) during the filtration tests. The feed water was collected from Mawson Lakes, South Australia, Australia, and 0.675 M NaCl was used as the draw solution. The feed water quality is summarised in Table 1. Both feed and draw solutions were maintained at 25°C using a cooling bath. The permeate water flux was (J_v) monitored using a digital balance (GF-6100, A&D Company, USA) which was connected to a PC. The equation is as follow:

$$J_v = \frac{\Delta V}{A\Delta t} \quad (1)$$

Table 1
The main composition of the feed solution

Feed water composition	Concentrations, mg/L
Total dissolved solids (TDS)	1,625.00
Dissolved organic carbon (DOC)	10.20
Al^{3+}	0.05
B^{3+}	0.98
Cu^{2+}	0.01
Fe^{3+}	0.02
Mn^{2+}	0.002
Ni^{2+}	0.004
Pb^{2+}	0.03
Si	4.15
Na^{+}	621.48
K^{+}	5.05
Mg^{2+}	44.89
Ca^{2+}	45.18
Cl^{-}	681.23
NO_2^{-}	26.58
SO_4^{2-}	264.20
NO_3^{-}	11.58

where ΔV is the volume change of the feed during the Δt (h) time and A is the effective membrane area (m^2). A conductivity meter (HQ40d, Hach, USA) was used to measure reverse salt flux (J_s) as follows:

$$J_s = \frac{C_t V_t - C_0 V_0}{A\Delta t} \quad (2)$$

where C_0 (g/L) and V_0 (L) are the initial concentration and initial volume of the feed solution, and C_t and V_t are the solutes concentration and the volume of the feed solution measured over a pre-determined Δt (h) time. A is the effective membrane area (m^2) [26].

In the present study, the active layer facing the draw solution (AL-DS) orientation was selected based on the results of our previous study [27]. It is known that the AL-DS orientation is more prone to fouling and that the fouling is less reversible than for the active layer facing the feed solution (AL-FS) orientation [3]. Our objective was to enhance the membrane performance and mitigate fouling on the membrane substrate layer which is more susceptible to fouling.

2.4. Fouling characterisations

After FO filtration experiments, the membrane coupons were taken out of the FO system and washed using MilliQ water, then the foulants on the pristine membrane and SNPM were analysed. Appropriate analytical techniques were employed for both samples in order to characterise the fouling mitigation by the SNP modified membrane. FESEM was used to examine the development of the fouling on the membrane surface. EDS was used for the elemental composition of the membrane foulants. ATR–FTIR was employed to identify the functional chemistry of the foulants on the membrane. The fluorescence spectrum of the foulants was obtained using a Hitachi F-2500 instrument (Hitachi, Japan). The fouled membrane was soaked in 50 mL of MilliQ water and sonicated using an ultra-sonicator (FS21H, Fisher Scientific, USA) for 2 min. The samples were filtered through a 0.45-μm filter before the measurement. The excitation wavelengths between 220 and 500 nm, emission wavelengths between 280 and 600 nm and a scanning speed of 1,500 nm/min were selected for this study. The spectrum of MilliQ water was used as a blank correction.

3. Results and discussion

3.1. Membrane surface characteristics

Fig. 1 shows the scanning electron microscopy (SEM) images and the corresponding EDS spectrum, and XPS scan survey data of the pristine and silica-coated membrane. The pristine TFC membrane surface (Fig. 1(a)) showed a cross-linked and embedded supporting layer structure. The EDS and XPS are used to determine the elemental composition in the membrane and the presence of the SNPs in the SNPM matrix. Three distinct peaks of carbon, oxygen and sulphur were observed from the pristine membrane surface (Fig. 1(a)). The membrane surface did not show significant change (Fig. 1(b)), although SNP deposition was evident as confirmed by the strong silicon peak in the EDS analysis shown in Fig. 1(b) and XPS scan data (the peak at binding energy of 103.61 eV ascribed to Si 2p) in Fig. 1(c) and Table 2. The oxygen peak and its atomic percentages became stronger in the SNPM compared with the pristine membrane. This also indicates the likely presence of SiO_2 [28]. EDS results are in good agreement with the XPS scan data for the pristine membrane. However, distinct differences observed in the case of SNPM. Recently, Gorzalski et al. [29] investigated the suitability of applying EDS and XPS for the elemental analysis of membrane surfaces. The differences in analysis depths by EDS (few microns) and XPS (< 10 nm) yielded the different elemental compositions between EDS and XPS data. It appears that both techniques are effective for detection of major elements in thick surface layers, but XPS is more effective at detecting major elements in this surface layers. Thus, in our case, both EDS and XPS are suitable at determining elemental composition of virgin PSF support layers, while XPS is preferable for the detection of thin SNPM surface coating layers.

The presence of SNPs on the membrane surface was further confirmed by ATR–FTIR. The FTIR spectra of the pristine membrane and SNPM are given in Fig. 2. The regions in the vicinity of 797 cm^{-1} (symmetric Si–O stretch) provide the evidence of SNP deposition. The Si–OH stretch peak in the vicinity of 950 cm^{-1} became higher after the surface modification [8,30]. The presence of these peaks in the spectrum of the SNPM confirmed the deposition of the SNPs on the membrane support layer. The functional groups –COOH and –OH of the PSF layers could react with silanol from the hydrolysed TEOS to bond via Si–O–C linkages. Another possible way to form a strong bond is via hydrogen bonding between silanol and –C=O groups on the PSF support layer (surface hydroxyl groups on SNPs through hydrogen bonding) [30,31].

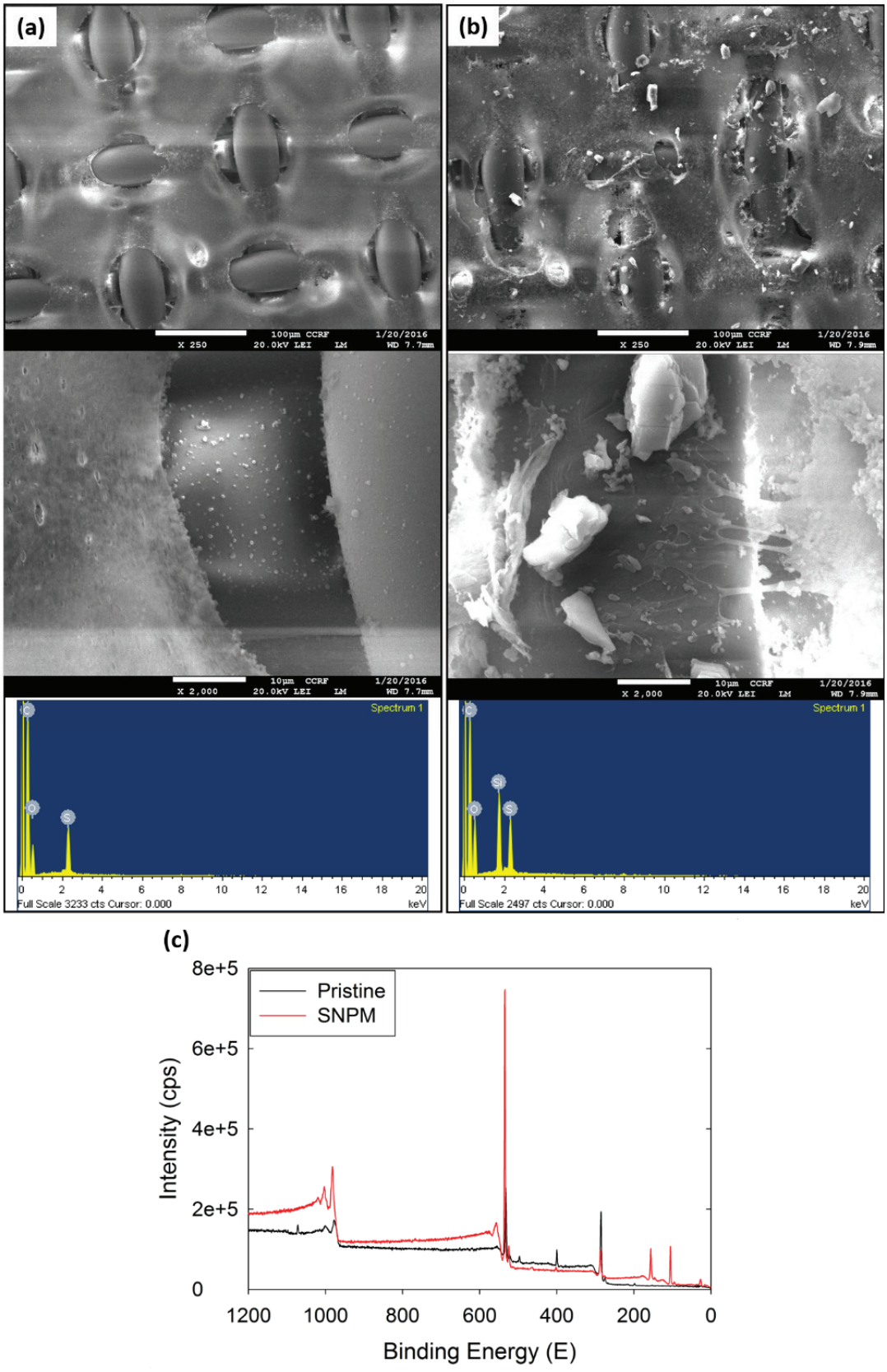

Fig. 1. FESEM images and corresponding EDS spectra of (a) pristine membrane, (b) SNPM, and (c) XPS survey scan data before and after the SNPs deposition.

The contact angle and zeta potential were measured to evaluate the physiochemical characteristics of the membrane and the results are summarised in Table 3. The contact angle was slightly decreased from 44.9° to 40.4° after the surface modification. The hydroxyl radicals on the surface of inorganic oxide nanoparticles enhanced the hydrophilic properties [22]. Given the limited operating pH of the commercial TFC membranes used in this study, the final pH of the coating solution was 2.2. This acidic coating solution produced oxygenated functional groups (–COOH, –OH and C=O) on the PSF support layer of the membrane. The resulting acid-oxidised membrane became hydrophilic [30]. The pH of the feed solution was 7.1. The zeta potential values at the operating pH of the feed solution were –13.2 and –12.4 mV for the pristine membrane and SNPM, respectively. Although a small decrease in zeta potential was observed after surface modification, this was considered insignificant.

The topography of the membrane was also examined and is presented in Fig. 3. It has been well documented that roughness has a significant impact on fouling behaviours [27,32,33]. Consistent porous structure is shown in the pristine TFC membrane support layer (Fig. 3(a)). The support/substrate layer of the membrane was smoothed after the deposition of the SNPs (Fig. 3(b)). The roughness value of the pristine membrane was 44.1 nm while this parameter decreased to 30.3 nm for the SNPM. The vertical scale (*Z*-axis) of the AFM images in Figs. 3(a) and (b) clearly showed the difference. They ranged from –400 to 100 nm for the pristine membrane and from –100 to 200 nm for the SNPM. The reduction in surface roughness after the surface modification was likely due to the preferentially immobilised SNPs within the valley-like regions, thus made the support layer smoother [34].

3.2. Filtration performance

The overall water flux patterns vs. operation time are shown in Fig. 4. The values were obtained by averaging the duplicated water permeation experiment results. A higher water flux was observed through the course of the filtration experiment by the SNPM compared with the pristine membrane. The permeate water flux of the SNPM was 5.1 LMH which is enhanced by 21.6% compared with that of the pristine membrane which yielded 4.0 LMH (Table 3). The enhanced wetting property of the membrane surface resulted in a higher permeate water flux across the membrane [35]. The flux through the pristine membrane constantly declined from the initial stage of the experiment, from 6 to 2 LMH. On the other hand, the flux decline for the SNPM was less severe than that of pristine membrane until 40 h and marked around 4 LMH at the end of the filtration experiments. The reverse salt flux was also enhanced after the coating procedure from 15.3 to 14.8 GMH (Table 3). This result indicates that the coating method enhanced the permeate water flux while maintaining the reverse salt flux rates. It is well known that hydrophilic and less charged membranes show higher water permeability and lower fouling propensity [17]. This is, in part, in good agreement with the present study. The roughness can be an important factor for determining material wettability [31]. The substantial decrease in the mean roughness factor (R_a) analysed

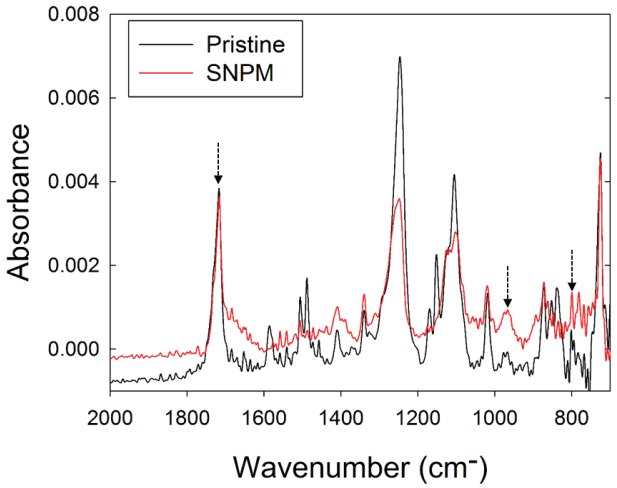

Fig. 2. FTIR spectra of the pristine membrane and SNPM.

Table 2
Elemental composition (atomic %) of the pristine membrane and SNPM by FESEM–EDS analysis and XPS survey scan

Sample	Method	C	O	S	Si
Pristine membrane	EDS	75.96 ± 0.09	22.57 ± 0.16	1.48 ± 0.06	–[a]
	XPS	73.78 ± 0.78	26.22 ± 2.03	–	–
SNPM	EDS	69.04 ± 0.61	27.34 ± 0.38	1.43 ± 0.09	2.19 ± 0.13
	XPS	23.49 ± 1.80	52.47 ± 0.56	–	24.04 ± 0.24

[a]Not detected.

Table 3
Physicochemical properties of the pristine and surface modified membranes

Membrane	Contact angle (°)	Zeta potential (mV) at pH 7.1	Roughness (nm)	Permeate water flux (L/m²·h (LMH))	Reverse salt flux (g/m²·h (GMH))
Pristine membrane	44.9 ± 1.9	–13.2 ± 0.7	44.1 ± 7.5	4.0	15.3 ± 4.8
SNPM	40.4 ± 2.7	–12.4 ± 2.5	30.3 ± 4.1	5.1	14.8 ± 1.8

by AFM images after the SNP coating increases membrane hydrophilicity, which in turn induces increased permeate water flux.

It can be postulated that the differences in the degree of water flux decline between the pristine membrane and SNPM are also caused by the lesser fouling rates of the SNPM. This will be discussed in section 3.3. It is known that when an ODMP is operated in AL-DS orientation, more complicated fouling occurs than in the AL-FS orientation due to the porous structure [13]. Normally, in the AL-DS orientation, the membrane possesses a high fouling propensity when the feed solution contains organic macromolecules or inorganic scalants that can penetrate into the porous support layer. When the porous support layer is clogged with foulants (internal fouling), this fouled/clogged porous support layer leads to enhanced ICP in the support layer and mass transfer resistance, and as a result, a sharp flux decline occurs [3,36]. This internal fouling is less reversible than the external fouling which mostly occurs in the AL-FS orientation while internal and external fouling occurs simultaneously in AL-DS orientation.

3.3. Enhanced antifouling property of SNPM

Fouling characterisations by the FESEM–EDS technique revealed that the pristine membrane was fouled by Al, Ca, Mg and Fe (Fig. 5(a) and Table 4). Trace amounts of Na and Cl were also detected. The coated membrane reduced fouling deposition on the membrane surface. Problematic scalants such as Ca and Mg can form intermolecular bridges with organic matter on the membrane surface and aggravate fouling [37]; however, both ions were not detected on the coated membrane. K and Fe were also not identified on the SNPM.

The fluorescence regional integration (FRI) method [38] was employed in order to analyse the fluorescence excitation–emission matrix (FEEM) characteristics of the fouling layers. The data obtained from the FEEM spectra also showed that SNPMs have antifouling properties. The FEEM spectra of the fouled pristine membrane are shown in Fig 6(a). Region IV was the pre-dominant peak, followed by Regions V and II. According to the FRI distribution of the membrane foulants, organic constituents are related to Regions IV, V and II. These are soluble microbial products, humic acid (HA) organics, and proteins with medium-to-high intensities and they are responsible for organic and biofouling. The fouling layer development was markedly reduced after the surface modification; only weak peaks of Region IV were found to be detected in the FEEM (Fig. 6(b)).

ATR–FTIR spectra of the pristine membrane and SNPM are shown in Fig. 7. The broad spectral bands of the foulants suggest that the feed solution contains various organic compounds with overlapping absorption bands [39]. The peak near 1,741 cm^{-1} may correspond to a carbonyl structure entity which is an indicator of organic fouling, possibly proteins [39]. The lower intensity in this region indicates that the degree of organic fouling substantially declined after the surface modification. Carboxylates typically absorb around 1,600 and 1,400 cm^{-1}, and amides typically absorb around 1,650 and 1,550 cm^{-1}. The vibrations around these regions result from the combination of amides and carbonyl groups which are some of the main components of dissolved organic matter [39]. The peaks

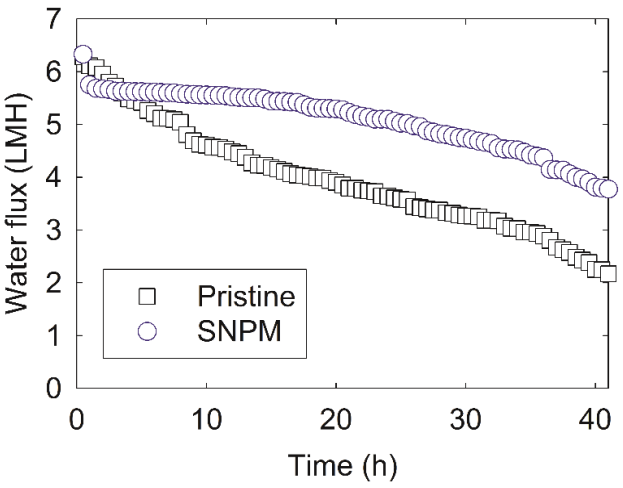

Fig. 4. Permeate water flux during the forward osmosis filtration.

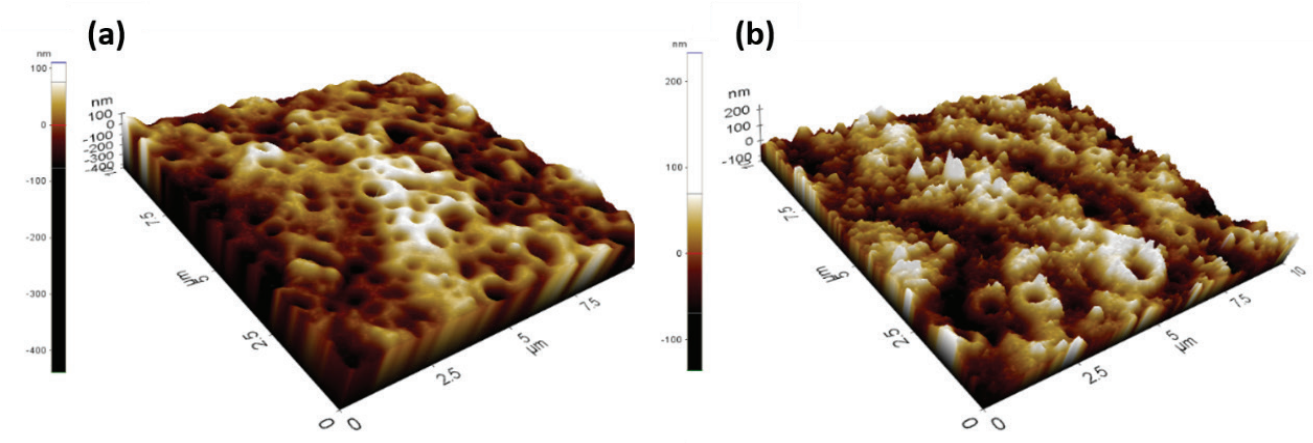

Fig. 3. AFM images of (a) pristine membrane and (b) SNPM.

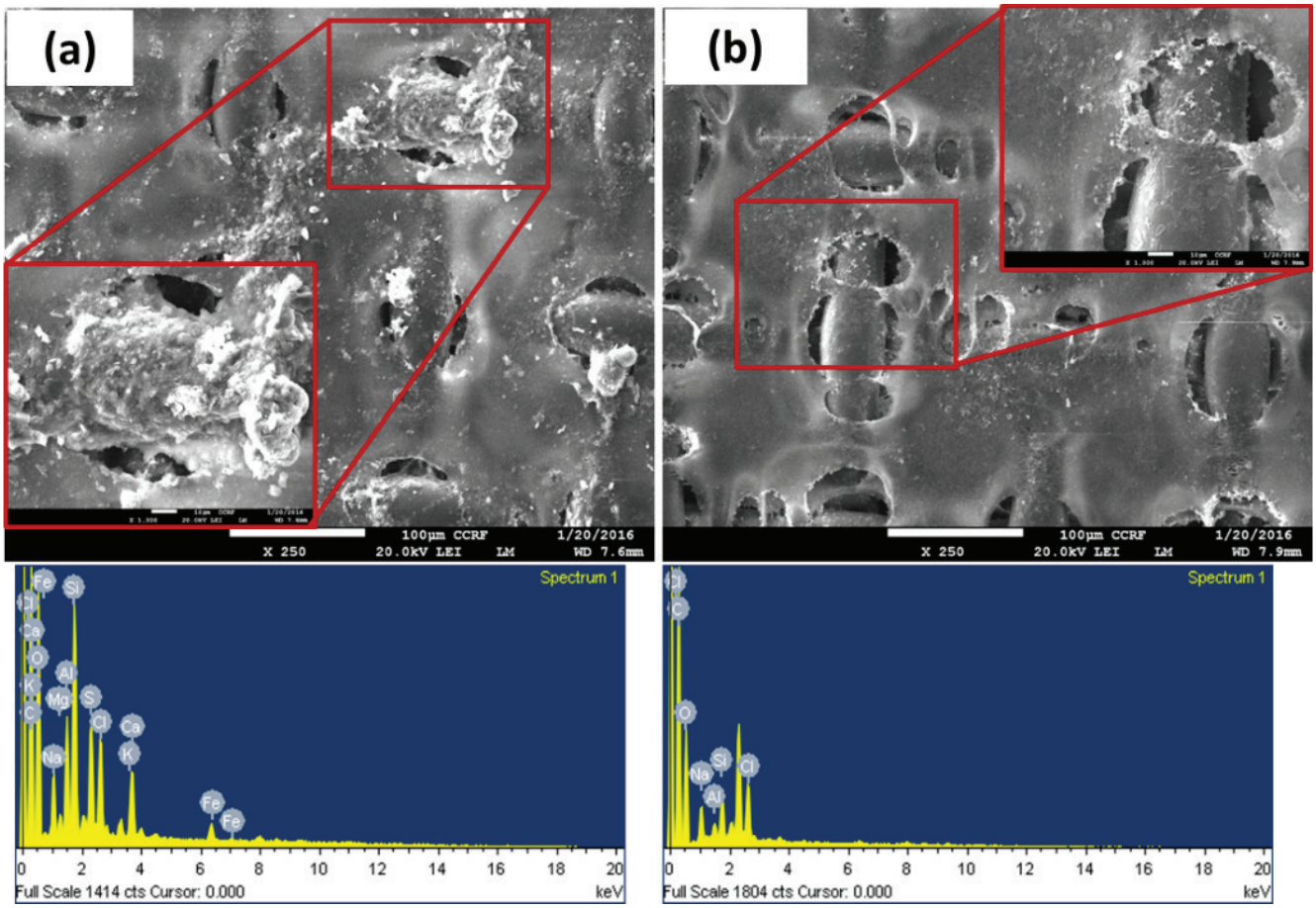

Fig. 5. FESEM images and corresponding EDS spectra of (a) the fouled pristine membrane and (b) the fouled SNPM.

Table 4
Elemental composition (atomic %) of fouled pristine membrane and SNPM samples by FESEM–EDS analysis

	Pristine membrane	SNPM
C	61.20 ± 0.96	69.92 ± 2.84
O	32.46 ± 0.57	25.90 ± 2.37
S	1.10 ± 0.15	1.71 ± 0.02
Si	1.46 ± 0.37	0.54 ± 0.14
Na	1.24 ± 0.07	1.08 ± 0.18
Cl	0.83 ± 0.01	0.68 ± 0.10
Al	0.83 ± 0.21	0.18 ± 0.07
Mg	0.22 ± 0.04	–[a]
K	0.12 ± 0.01	–
Ca	0.61 ± 0.09	–
Fe	0.07 ± 0.05	–

[a]Not detected.

near 1,340 and 1,250 cm^{-1} might be due to the presence of methyl and C–O bond (ester) entities, respectively [40]. The peaks at 1,100 cm^{-1} are possibly arise from polysaccharides which prevalent from a membrane process treating relatively hydrophilic natural organic matter-source water [41]. The peak in the vicinity of 1,034 cm^{-1} is due to absorption of the silicate impurities in HA organics [39]. It can be clearly observed that the intensities of masked peaks are diminished after the surface modification. This indicates that the organic fouling was mitigated by the surface modification by SNPs.

As described in the earlier sections, membranes with the rougher surface and elevated regions (ridge- and valley-like structure) had greater membrane surface area and more active sites for foulant deposition [8]. Increased hydrophilicity of the membrane surfaces provides higher affinity to water, as a result, creating fouling resistance. In addition, use of neutrally charged nanoparticles or nanoparticles containing certain functional groups that can minimise interaction with foulants (i.e., zwitterionic compounds against protein foulants) at the membrane surface could be beneficial [35]. In our case, smoothened membrane surface and enhanced hydrophilicity were the key mechanisms that help mitigating fouling adsorption.

4. Conclusions

In this study, a facile dip-coating process involving SNPs in sol–gel was employed to modify the FO membranes in order to enhance their performance. SEM–EDS, XPS and ATR–FTIR confirmed the successful deposition of SNPs on the membrane substrate layers for the AL-DS orientation. The modification has caused changes of the membrane surface

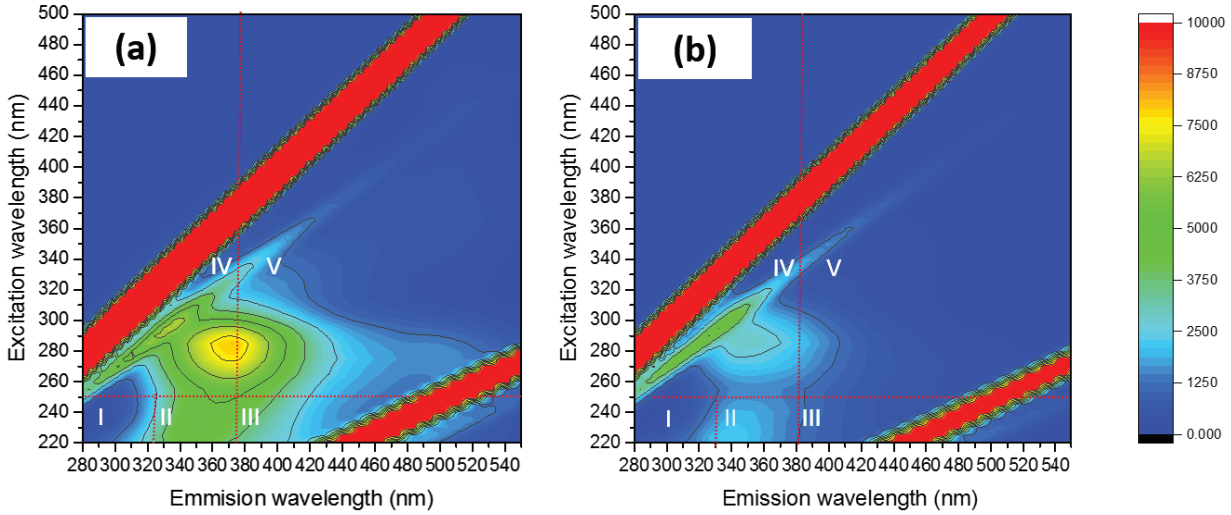

Fig. 6. Fluorescence excitation–emission spectra of the foulants from the (a) pristine membrane and (b) SNPM samples. Regions I (Ex/Em = 200–250/280–330) and II (Ex/Em=200–250/330–380) are correspond to simple amino acid moieties-like tyrosine and tryptophan (P1 and P2). Region III (Ex/Em = 200–260/380–500) is attributed to fulvic acid-like (FA) material. Region IV (Ex/Em = 250–280/310–380) is closely related to soluble microbial product (SMP), while Region V (Ex/Em = 280–380/380–500) is related to humic acid (HA) organics.

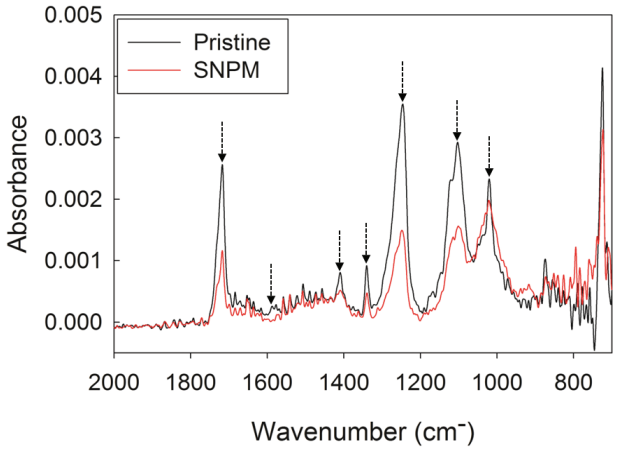

Fig. 7. FTIR spectra of the fouled pristine membrane and SNPM samples.

properties in favour of enhanced permeate water flux and antifouling property. These results were achieved by making it more hydrophilic and smoother than the pristine membrane. It can be concluded that the SNPM is more resistant to fouling compared with the pristine TFC FO membrane. A further study using the current membrane surface modification method would be beneficial in treating challenging feed waters with high fouling potential, especially biofouling, for reduced fouling control.

Acknowledgements

The authors would like to acknowledge the financial support of the National Centre of Excellence in Desalination Australia, which is funded by the Australian Government through the 'Water for the Future' initiative. This research was partly supported by a grant (16IFIP-B088091-03) from the Industrial Facilities & Infrastructure Research Program funded by the Ministry of Land, Infrastructure and Transport of the Korean Government. The authors also wish to thank the School of Natural and Built Environments and the University of South Australia for providing the PhD scholarship.

References

[1] T.Y. Cath, A.E. Childress, M. Elimelech, Forward osmosis: principles, applications, and recent developments, J. Membr. Sci., 281 (2006) 70–87.
[2] S. Zhao, L. Zou, C.Y. Tang, D. Mulcahy, Recent developments in forward osmosis: opportunities and challenges, J. Membr. Sci., 396 (2012) 1–21.
[3] Q. She, R. Wang, A.G. Fane, C.Y. Tang, Membrane fouling in osmotically driven membrane processes: a review, J. Membr. Sci., 499 (2016) 201–233.
[4] Y. Chun, F. Zaviska, E. Cornelissen, L. Zou, A case study of fouling development and flux reversibility of treating actual lake water by forward osmosis process, Desalination, 357 (2015) 55–64.
[5] Y. Chun, F. Zaviska, S.-J. Kim, D. Mulcahy, E. Yang, I.S. Kim, L. Zou, Fouling characteristics and their implications on cleaning of a FO-RO pilot process for treating brackish surface water, Desalination, 394 (2016) 91–100.
[6] B.-H. Jeong, E.M.V. Hoek, Y. Yan, A. Subramani, X. Huang, G. Hurwitz, A.K. Ghosh, A. Jawor, Interfacial polymerization of thin film nanocomposites: a new concept for reverse osmosis membranes, J. Membr. Sci., 294 (2007) 1–7.
[7] G.L. Jadav, P.S. Singh, Synthesis of novel silica-polyamide nanocomposite membrane with enhanced properties, J. Membr. Sci., 328 (2009) 257–267.
[8] A. Sabir, M. Shafiq, A. Islam, F. Jabeen, A. Shafeeq, A. Ahmad, M.T. Zahid Butt, K.I. Jacob, T. Jamil, Conjugation of silica nanoparticles with cellulose acetate/polyethylene glycol 300 membrane for reverse osmosis using $MgSO_4$ solution, Carbohydr. Polym., 136 (2016) 551–559.
[9] Y. Yang, H. Zhang, P. Wang, Q. Zheng, J. Li, The influence of nano-sized TiO_2 fillers on the morphologies and properties of PSF UF membrane, J. Membr. Sci., 288 (2007) 231–238.
[10] S.-J. Kim, P.-S. Lee, S. Bano, Y.-I. Park, S.-E. Nam, K.-H. Lee, Effective incorporation of TiO_2 nanoparticles into polyamide thin-film composite membranes, J. Appl. Polym. Sci., 133 (2016) 43383.

[11] H.-L. Yang, J.C.-T. Lin, C. Huang, Application of nanosilver surface modification to RO membrane and spacer for mitigating biofouling in seawater desalination, Water Res., 43 (2009) 3777–3786.
[12] A. Nguyen, L. Zou, C. Priest, Evaluating the antifouling effects of silver nanoparticles regenerated by TiO_2 on forward osmosis membrane, J. Membr. Sci., 454 (2014) 264–271.
[13] X. Liu, L.-X. Foo, Y. Li, J.-Y. Lee, B. Cao, C.Y. Tang, Fabrication and characterization of nanocomposite pressure retarded osmosis (PRO) membranes with excellent anti-biofouling property and enhanced water permeability, Desalination, 389 (2016) 137–148.
[14] L. Yan, S. Hong, M.L. Li, Y.S. Li, Application of the Al_2O_3–PVDF nanocomposite tubular ultrafiltration (UF) membrane for oily wastewater treatment and its antifouling research, Sep. Purif. Technol., 66 (2009) 347–352.
[15] M. Ben-Sasson, X. Lu, E. Bar-Zeev, K.R. Zodrow, S. Nejati, G. Qi, E.P. Giannelis, M. Elimelech, In situ formation of silver nanoparticles on thin-film composite reverse osmosis membranes for biofouling mitigation, Water Res., 62 (2014) 260–270.
[16] C. Dong, G. He, H. Li, R. Zhao, Y. Han, Y. Deng, Antifouling enhancement of poly(vinylidene fluoride) microfiltration membrane by adding $Mg(OH)_2$ nanoparticles, J. Membr. Sci., 387–388 (2012) 40–47.
[17] G.-d. Kang, Y.-m. Cao, Development of antifouling reverse osmosis membranes for water treatment: a review, Water Res., 46 (2012) 584–600.
[18] D. Wang, G.P. Bierwagen, Sol–gel coatings on metals for corrosion protection, Prog. Org. Coat., 64 (2009) 327–338.
[19] M. Ben-Sasson, X. Lu, S. Nejati, H. Jaramillo, M. Elimelech, In situ surface functionalization of reverse osmosis membranes with biocidal copper nanoparticles, Desalination, 388 (2016) 1–8.
[20] X.Q. Zhang, L.H. Yin, M. Tang, Y.P. Pu, ZnO, TiO_2, SiO_2, and Al_2O_3 nanoparticles-induced toxic effects on human fetal lung fibroblasts, Biomed. Environ. Sci., 24 (2011) 661–669.
[21] S. Manzo, S. Buono, G. Rametta, M. Miglietta, S. Schiavo, G. Di Francia, The diverse toxic effect of SiO_2 and TiO_2 nanoparticles toward the marine microalgae *Dunaliella tertiolecta*, Environ. Sci. Pollut. Res., 22 (2015) 15941–15951.
[22] L.Y. Ng, A.W. Mohammad, C.P. Leo, N. Hilal, Polymeric membranes incorporated with metal/metal oxide nanoparticles: a comprehensive review, Desalination, 308 (2013) 15–33.
[23] H. Wu, B. Tang, P. Wu, Development of novel SiO_2–GO nanohybrid/polysulfone membrane with enhanced performance, J. Membr. Sci., 451 (2014) 94–102.
[24] X. Liu, H.Y. Ng, Fabrication of layered silica–polysulfone mixed matrix substrate membrane for enhancing performance of thin-film composite forward osmosis membrane, J. Membr. Sci., 481 (2015) 148–163.
[25] C.-M. Kim, S.-J. Kim, L.H. Kim, M.S. Shin, H.-W. Yu, I.S. Kim, Effects of phosphate limitation in feed water on biofouling in forward osmosis (FO) process, Desalination, 349 (2014) 51–59.
[26] H.T. Nguyen, N.C. Nguyen, S.-S. Chen, H.H. Ngo, W. Guo, C.-W. Li, A new class of draw solutions for minimizing reverse salt flux to improve forward osmosis desalination, Sci. Total Environ., 538 (2015) 129–136.
[27] Y. Chun, S.-J. Kim, G.J. Millar, D. Mulcahy, I.S. Kim, L. Zou, Forward osmosis as a pre-treatment for treating coal seam gas associated water: flux and fouling behaviours, Desalination, 403 (2017) 144–152.
[28] M. Kanungo, H.S. Isaacs, S.S. Wong, Quantitative control over electrodeposition of silica films onto single-walled carbon nanotube surfaces, J. Phys. Chem. C, 111 (2007) 17730–17742.
[29] A.S. Gorzalski, C. Donley, O. Coronell, Elemental composition of membrane foulant layers using EDS, XPS, and RBS, J. Membr. Sci., 522 (2017) 31–44.
[30] Y. Yang, S. Qiu, W. Cui, Q. Zhao, X. Cheng, R.K.Y. Li, X. Xie, Y.-W. Mai, A facile method to fabricate silica-coated carbon nanotubes and silica nanotubes from carbon nanotubes templates, J. Membr. Sci., 44 (2009) 4539–4545.
[31] X. Lin, M. Yang, H. Jeong, M. Chang, J. Hong, Durable superhydrophilic coatings formed for anti-biofouling and oil–water separation, J. Membr. Sci., 506 (2016) 22–30.
[32] M. Elimelech, Z. Xiaohua, A.E. Childress, H. Seungkwan, Role of membrane surface morphology in colloidal fouling of cellulose acetate and composite aromatic polyamide reverse osmosis membranes, J. Membr. Sci., 127 (1997) 101–109.
[33] G. Chen, Z. Wang, L.D. Nghiem, X.-M. Li, M. Xie, B. Zhao, M. Zhang, J. Song, T. He, Treatment of shale gas drilling flowback fluids (SGDFs) by forward osmosis: membrane fouling and mitigation, Desalination, 366 (2015) 113–120.
[34] A. Tiraferri, Y. Kang, E.P. Giannelis, M. Elimelech, Highly hydrophilic thin-film composite forward osmosis membranes functionalized with surface-tailored nanoparticles, ACS Appl. Mater. Interfaces, 4 (2012) 5044–5053.
[35] A. Tiraferri, Y. Kang, E.P. Giannelis, M. Elimelech, Superhydrophilic thin-film composite forward osmosis membranes for organic fouling control: fouling behavior and antifouling mechanisms, Environ. Sci. Technol., 46 (2012) 11135–11144.
[36] C.Y. Tang, Q. She, W.C.L. Lay, R. Wang, A.G. Fane, Coupled effects of internal concentration polarization and fouling on flux behavior of forward osmosis membranes during humic acid filtration, J. Membr. Sci., 354 (2010) 123–133.
[37] S. Zou, Y. Gu, D. Xiao, C.Y. Tang, The role of physical and chemical parameters on forward osmosis membrane fouling during algae separation, J. Membr. Sci., 366 (2011) 356–362.
[38] W. Chen, P. Westerhoff, J.A. Leenheer, K. Booksh, Fluorescence excitation–emission matrix regional integration to quantify spectra for dissolved organic matter, Environ. Sci. Technol., 37 (2003) 5701–5710.
[39] K.J. Howe, K.P. Ishida, M.M. Clark, Use of ATR/FTIR spectrometry to study fouling of microfiltration membranes by natural waters, Desalination, 147 (2002) 251–255.
[40] Z. Wang, Z. Wu, X. Yin, L. Tian, Membrane fouling in a submerged membrane bioreactor (MBR) under sub-critical flux operation: membrane foulant and gel layer characterization, J. Membr. Sci., 325 (2008) 238–244.
[41] J. Cho, G. Amy, J. Pellegrino, Y. Yoon, Characterization of clean and natural organic matter (NOM) fouled NF and UF membranes, and foulants characterization, Desalination, 118 (1998) 101–108.